

## Fermi surfaces of the two-dimensional surface states on vicinal Cu(111)

F. Baumberger, T. Greber, and J. Osterwalder

*Physik-Institut, Universität Zürich, Winterthurerstrasse 190, CH-8057 Zürich, Switzerland*

(Received 23 February 2001; published 26 October 2001)

The Shockley ( $L$ -gap) surface states on Cu(111) and the vicinal (332) and (221) surfaces have been mapped by angle-scanned ultraviolet photoelectron spectroscopy. We find two-dimensional (2D) surface states on both vicinal surfaces. An analysis of the photoemission line shape that includes the effects of the terrace width distribution indicates an isotropic reduction of the photohole lifetime on the vicinal surfaces and allows us to quantify the intrinsic initial-state dispersion. For the larger step-step separation of 12 Å on Cu(332), the Fermi contour shows the characteristic elliptical shape of a 2D Bloch state in a 1D lattice. On Cu(221) with 7.7 Å terraces we find an isotropic dispersion within the accuracy of the experiment. These findings are interpreted as a continuous surface state to surface resonance transition with decreasing terrace length. The effective step potential is estimated using a simple perturbation theory ansatz.

DOI: 10.1103/PhysRevB.64.195411

PACS number(s): 73.20.At, 71.18.+y, 79.60.-i

### I. INTRODUCTION

Vicinal surfaces are miscut by a small angle relative to a high-symmetry crystal plane and thus generally composed of low-index terraces bounded by steps with a preferential orientation. The motivation for the study of these surfaces comes from various quarters. Structural aspects are widely investigated, since the energetics of a monoatomic step on an otherwise perfect crystal surface are fundamental for surface morphology.<sup>1</sup> The enhanced catalytic activity of step sites makes vicinal surfaces attractive model systems in heterogeneous catalysis.<sup>2,3</sup> Stepped surfaces are also of increasing importance as functional substrates for the growth of new low-dimensional solids with tailored electronic properties.<sup>4,5</sup>

Vicinal Cu(111) surfaces are of specific interest due to the presence of a free-electron-like Shockley surface state on the corresponding flat surface.<sup>6–8</sup> This state arises as a consequence of the broken translational symmetry along the surface normal. Its wave function is confined perpendicular to the surface by the surface potential step and the crystal band gap.<sup>9</sup> In the surface plane it propagates free-electron-like with a Fermi wavelength of  $\lambda_F \sim 3$  nm. Despite its low density—one electron is shared by about 20 surface atoms—this state is of high interest due to its energetic position crossing the Fermi level. Scattering of surface state electrons at nanostructures thus modulates the local density of states (DOS) at the Fermi level.<sup>10</sup> Recently it has been observed that this modulation is strong enough to produce a feedback on the atomic arrangement.<sup>11</sup>

Modifications of the Shockley surface state on stepped surfaces have been studied in a number of works.<sup>12–16</sup> Momentum-resolved photoemission experiments showed a propagating two-dimensional (2D) state, shifted in energy and momentum with respect to the flat surface. From the momentum shift of the band bottom it was concluded that the surface state propagates along the average surface plane rather than on the individual terraces.<sup>13</sup> Recent experiments of Ortega *et al.*, however, indicated a critical terrace length of  $\sim 17$  Å above which the electron wave function switches from step modulation to terrace modulation.<sup>15</sup> The latter was observed earlier by scanning tunneling microscopy on large

terraces.<sup>10</sup> The shift of the surface state band towards higher kinetic energies was interpreted in terms of a 1D Kronig-Penney model,<sup>14</sup> mimicking the steps as a periodic array of repulsive  $\delta$ -function potentials. However, an unambiguous manifestation of a periodic potential is given only by a changed effective band mass or the opening of a band gap at the superlattice zone boundary. The energy shift may be caused as well by a homogeneous potential shift as it is, e.g., observed upon cooling of the surface.<sup>17</sup>

To our knowledge the opening of a superlattice gap has not been reported so far for the Shockley surface state in contrast to the observed superlattice periodicity for a Tamm state<sup>18</sup> and an image potential state<sup>19</sup> on vicinal Cu(100). It is thus still an open issue whether the long-range modulation of the atomic potential caused by the steps is strong enough to result in distinct superlattice effects on the Shockley-type surface state. In contrast to Tamm states which are essentially localized in the outermost atomic layer, Shockley-type surface states exhibit a considerable bulk penetration depth. This obviously reduces the sensitivity to the step potentials and will be reflected in a 1D model by a smaller corrugation of the *effective* potential landscape. For terrace lengths of only a few atomic rows we also expect that step-step interaction smoothes the potential barriers. With increasing miscut away from the [111] direction, surface and bulk wave functions can hybridize to a surface resonance, giving rise to an increasing decay length towards the bulk. Surface-bulk coupling can in principle be measured via the photoemission linewidth, reflecting the lifetime of the excited hole state. Sánchez *et al.* reported a considerable increase in the surface state linewidth with decreasing terrace length.<sup>14</sup> However, we are not aware of any attempt to deduce lifetimes of the excited hole state.

In this paper we present a detailed study of the band dispersion on two vicinal surfaces with terrace lengths  $l < \lambda_F/2$  where the surface state band is unoccupied at the superlattice zone boundaries. With a careful data analysis using an appropriate model for the photoemission line shape we gain new insight concerning surface state confinement on vicinal Cu(111). By measuring the full surface state Fermi surfaces we find a significant deviation from a free-

electron-like behavior in the case of Cu(332). This is strong evidence for the superlattice sensitivity of the surface state and can be used to estimate the effective potential strength. Our line shape analyses indicate a highly reduced lifetime of the photohole, consistent with the expected surface state to surface resonance transition.

## II. EXPERIMENT

Angle-scanned ultraviolet photoemission spectroscopy (ARUPS) data and in particular Fermi surface maps (FSM) generally exhibit two rather different types of features, the relative importance of which depends on the damping of the electron in its final state.<sup>20,21</sup> For a large damping and a correspondingly small inelastic mean free path, the photoemission intensity is essentially proportional to the 1D density of initial states, associated with the  $k_{\perp}$  dispersion at a given  $k_{\parallel}$ .<sup>21</sup> The resulting homogeneous intensity distribution may be viewed as a surface projection of the initial-state constant energy surface. For a large mean free path, on the other hand, the photoemission intensity originates from direct transitions to unoccupied final states. The corresponding features in a FSM are well-defined lines of high intensity, representing the initial-state Fermi surface along the  $k$ -space contour of the final state. These lines are typically 10 times more intense than the above-mentioned DOS-derived features and will be mainly interpreted in the present paper. For most cases the assumption of a free-electron final state proved to be sufficient.<sup>20,22</sup> This interpretation scheme of photoemission data is illustrated in Fig. 1. A quasiparticle peak in the photoemission spectrum can be observed when initial and final states intersect in  $k$ -space. The double peak between  $\bar{\Gamma}_{00}$  and  $\bar{\Gamma}_{10}$  can therefore be assigned to the Fermi level crossing of the Shockley surface state, whereas the weaker features on the left originate from the  $sp$ -derived bulk Fermi surface. The initial-state momentum can be calculated from the electron emission angle and kinetic energy. For uniform work-function  $\Phi$  and inner potential diffraction of the outgoing electron wave conserves the momentum component in the surface plane:

$$(k_x, k_y) = \frac{1}{\hbar} \sqrt{2m_e E_{kin}^{vac}} (\sin \theta \cos \phi, \sin \theta \sin \phi), \quad (1)$$

where  $E_{kin}^{vac} = h\nu - E_B - \Phi$  is the kinetic energy with respect to the vacuum level,  $\theta$  the polar and  $\phi$  the azimuthal emission angle. The electron binding energy  $E_B$  equals zero at the Fermi level.

The experiments were performed in a VG ESCALAB 220 photoelectron spectrometer, modified with a computer-controlled two-axis sample goniometer.<sup>23</sup> The monochromatized UV radiation from a He discharge lamp is weakly  $p$  polarized due to the reflection on the monochromator grating. Its oblique incidence can cause different intensities for  $k$  points which are equivalent with respect to the crystal symmetry.<sup>24</sup> All photoemission data were taken with He I $\alpha$  radiation (21.22 eV) at room temperature. The resolution parameters were set to  $\Delta E < 40$  meV and  $\Delta \theta < 0.8^\circ$  [full width at half maximum (FWHM)].

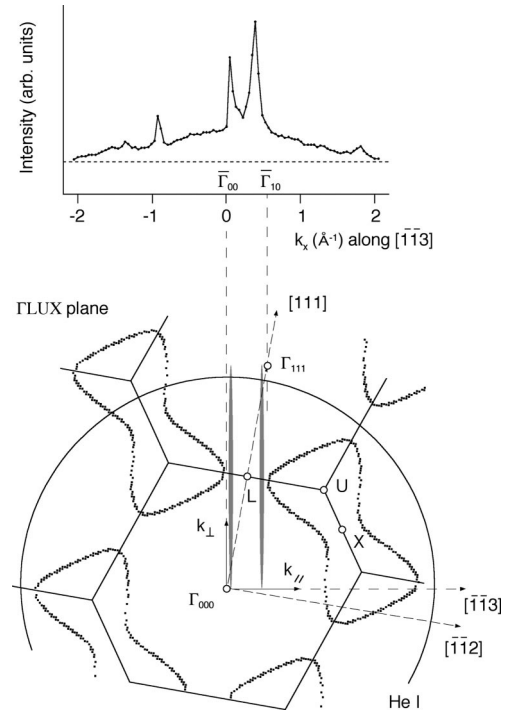


FIG. 1. Interpretation scheme for an angle-scanned photoemission experiment. The top of the figure shows the measured photoemission intensity at the Fermi level of Cu(332) for various emission angles in the  $(1\bar{1}0)$  symmetry plane (perpendicular to the steps and the surface). Below the  $(1\bar{1}0)$  plane is shown in the extended zone scheme. Calculated initial states on the bulk Fermi surface are shown partly dotted; the surface-state Fermi surface is represented by the two rods near the  $L$  point. The large circle around  $\Gamma_{000}$  shows the final-state sphere for excitation with He I radiation.

Hard-sphere models of the investigated vicinal surfaces are shown in Fig. 2. All surfaces are vicinal to the close-packed  $(111)$  surface and exhibit monoatomic steps with  $(11\bar{1})$  microfacets. This results in terrace widths of  $n + 1/3$  atomic rows, where  $n$  equals 5 for Cu(332) and 3 for the  $(221)$  surfaces, respectively. The nominal miscut angles relative to  $[111]$  are  $10.0^\circ$  (332) and  $15.8^\circ$  (221).

The single-crystal samples (Mateck, Jülich) were polished mechanically to within  $< 0.5^\circ$  accuracy, before inserting them in the UHV system. For the initial *in situ* preparation repeated cycles of low-energy ( $\sim 200$  eV) Ar-ion sputtering followed by annealing with temperatures subsequently increasing to 950 K were used. After this treatment mild annealing to  $\sim 525$  K proved to be sufficient to remove sputter damage.

The crystallographic directions were checked *in situ* by x-ray photoelectron diffraction (XPD) with an accuracy of better than  $1^\circ$ . Miscut angles were determined from a comparison of the crystallographic directions with laser reflection at the macroscopic surface. Surface order was checked by scanning tunneling microscopy (STM) and low-energy electron diffraction (LEED). Terrace width distributions  $P(l)$  were deduced from an analysis of the LEED spot profiles using the formalism given in Ref. 25. The average terrace widths of  $\langle l \rangle^{332} = 12.7 \pm 1.0$  Å and  $\langle l \rangle^{221} = 7.0 \pm 0.5$  Å

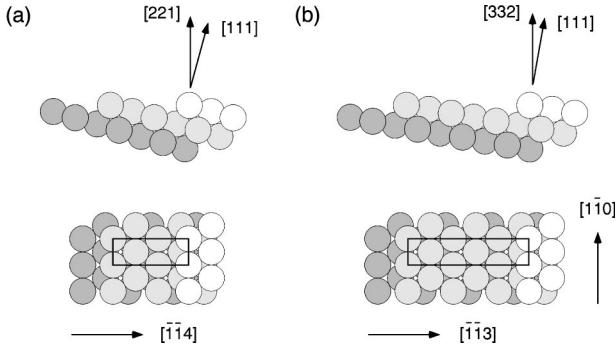


FIG. 2. Nominal surface atomic configurations for (a) Cu(221) and (b) Cu(332). Primitive surface unit cells are indicated by rectangles. Step-step separations  $l$  and miscut angles  $\alpha$  relative to  $[111]$  are  $l^{(332)} = 12 \text{ \AA}$ ,  $\alpha^{(332)} = 10^\circ$ , and  $l^{(221)} = 7.7 \text{ \AA}$ ,  $\alpha^{(221)} = 15.8^\circ$ , respectively.

agree with the nominal values and the miscut angles as determined by XPD. Standard deviations  $\sigma_l$  of  $P(l)$  are calculated from the spot widths. Without any resolution corrections we obtain  $\sigma_l = 0.37\langle l \rangle$  as an upper limit for both samples, close to the value found in a STM study ( $\sigma_l = 0.26\langle l \rangle$ ).<sup>26</sup> Sample cleanliness was verified by x-ray photoelectron spectroscopy (XPS). The contamination levels during the experiments were always below 0.04 ML carbon and 0.02 ML oxygen.

### III. RESULTS AND DISCUSSION

#### A. Experimental data

The bulk electronic structure of Cu near the Fermi level is dominated by the free-electron-like dispersing  $sp$ -band, crossing the Fermi level at  $k_F \sim 1.4 \text{ \AA}^{-1}$ . As a consequence of the lattice periodicity the  $sp$  band is back folded at the  $L$  points of the Brillouin zone and gaps at the Fermi level open along  $\langle 111 \rangle$ , giving rise to the characteristic necks in the Fermi surface. These  $L$  gaps support the investigated Shockley surface state on Cu(111) and its analog on the vicinal surfaces. The necks of the bulk Fermi surface as well as the bone shaped hole orbits are readily identified as direct transition lines in the Fermi surface map from Cu(332) shown in Fig. 3. The bright elliptical feature near  $\bar{\Gamma}$  is the Shockley surface state. The Fermi level crossing of the bulk bands is measured at  $k_{\parallel}$  values corresponding to a projection of the initial state onto a (332) plane. This confirms that  $k_{\parallel}$  is conserved with respect to the average surface plane, rather than the terrace plane. In agreement with earlier studies<sup>27</sup> we have no indications for effects of the step structure on the location of the bulk bands. The contour of the DOS-derived feature is indicated by a thin semicircle. It appears distinctly shifted from the direct transition lines and shows no clear indication of the  $L$  gap. This behavior is readily interpreted within the frame work presented in Ref. 21. The rather sharp boundary of the DOS-derived feature results from the edge of the projected first Fermi sphere and thus gives the cross section of the initial state Fermi surface within a (332) plane passing through the zone center. The absence of any dark spot in the DOS-like feature indicates that initial states are available for

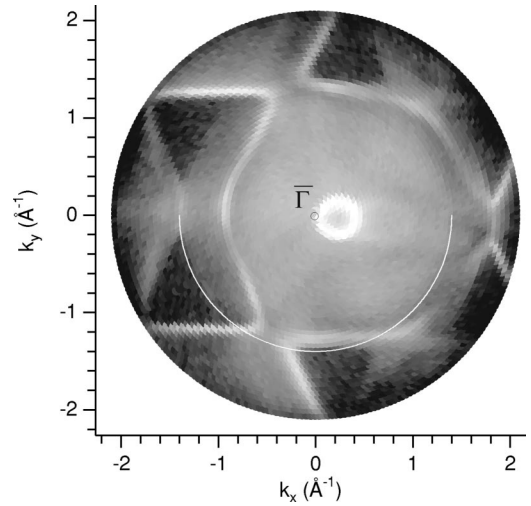


FIG. 3. He I excited Fermi surface map from Cu(332), displayed on a logarithmic gray scale. The bone-shaped direct transition lines represent a cut through the bulk Fermi surface. The bright ellipse near  $\bar{\Gamma}$  is the  $L$ -gap surface-state. The semicircle with radius  $1.40 \text{ \AA}^{-1}$  approximates the DOS-like feature in the lower half of the plot.

all values of  $k_{\parallel}$  i.e., that there is no remnant gap in the projected bulk band structure as is, in contrast, observed in the FSM from Cu(111) (Fig. 4).

In the following we focus on the  $k$ -space region of the Shockley surface state. We choose  $k$ -space coordinates with  $k_x$  normal to the steps, running upstairs for positive values, and  $k_y$  parallel to the steps. Fermi surface maps with high sampling density ( $\sim 8000$  angular settings) from all three crystal faces are shown in Fig. 4. To enhance weaker features we displayed the photoemission intensity on a logarithmic gray scale as a function of  $k_{\parallel}$  for  $\theta < 30^\circ$  or  $k_{\parallel} < 1.05 \text{ \AA}^{-1}$ . The surface state Fermi contour for Cu(111) in Fig. 4(a) is centered at  $\bar{\Gamma}$  and perfectly circular as expected for a 2D free-electron gas. Its Fermi wave vector of  $k_F = 0.205 \text{ \AA}^{-1}$  is well inside the projected bulk band gap ( $k_{neck} = 0.26 \text{ \AA}^{-1}$ ) and results in an occupation of  $\langle n \rangle^{(111)} = 0.037e^-/\text{surface atom}$ . The measured linewidth of  $0.026 \text{ \AA}^{-1}$  is dominated by the angular resolution. The broad threefold symmetric structure at higher  $k_{\parallel}$  values is well reproduced by calculations and seems to be remnant from direct transitions to non-free-electron-like final states.<sup>21</sup> The projected  $L$  gap is clearly visible as a black spot around  $\bar{\Gamma}$ .

The Fermi contours from the vicinal samples appear shifted by half a reciprocal lattice vector from  $\bar{\Gamma}_{00}$  to  $\bar{M}_{1/2,0}$ , the projection of the supporting  $L_{1/2,1/2,1/2}$  point. Invoking the interpretation scheme as illustrated in Fig. 1 this shift requires that the surface state wave function is dispersionless along  $k_{\perp}$  and thus decays in real space perpendicular to the average surface, rather than along the terrace normal. As a consequence the surface state propagates along the average surface as it was found in earlier studies.<sup>13</sup> This has two important consequences. First, a wave function extending in  $k$ -space along the surface normal gradually separates from

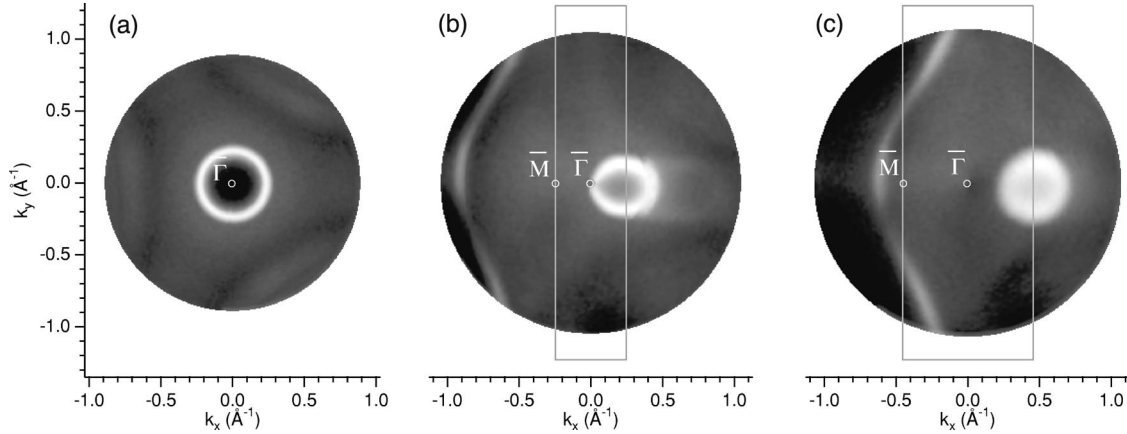


FIG. 4. Fermi surface maps of Cu(111) (a), Cu(332) (b), and Cu(221) (c). Superlattice Brillouin zones and the high-symmetry points  $\bar{\Gamma}_{00}$  and  $\bar{M}_{\bar{1}\bar{2},0}$  are overlaid. The photoemission intensity is displayed as a function of parallel momentum on a logarithmic gray scale ranging from black at minimum intensity to white at maximum intensity.

the gap which extends along  $[111]$ . The surface state will thus hybridize with bulk states and should more correctly be termed a surface resonance. This will certainly reduce the photohole lifetime. To what extent the enhanced linewidth may be attributed to this effect will be discussed in the next section. As a second point the propagation along the average surface indicates a coherent interaction of the initial-state wave function over several terraces. We can thus expect the surface state to react to the step potentials in a similar way as a Bloch state. This is unambiguously observed in the Fermi surface map from Cu(332) in Fig. 4(b). The elliptical Fermi contour with its larger spanning vector perpendicular to the steps indicates the enhanced effective mass for a propagation in the periodic step lattice. In the same figure we identify faint lines starting from the ellipsoidal feature to the right. These features reflect a 1D Fermi surface with Fermi wave vectors  $k_F^{1D} = \pm 0.17 \text{ \AA}^{-1}$  independent of the momentum  $k_x$  perpendicular to the steps. The corresponding step-induced 1D state was discussed in more detail in a previous publication.<sup>16</sup> An analogous state is not found in the Fermi surface map of Cu(221) shown in Fig. 4(c). In contrast to the (332) surface, the 2D surface-state on Cu(221) is again very close to the isotropic Fermi surface of a free-electron gas.

Surface state dispersion plots along  $\bar{\Gamma}\bar{M}$  are shown in Fig. 5. The data are normalized with a Fermi-Dirac distribution

function and mapped to  $k_x$  using Eq. (1). The instrumental Fermi edge was determined on a polycrystalline silver sample. In order to reduce background noise far above the Fermi level an offset of 2 per mill has been added to the Fermi function. The dispersion plot measured for Cu(111) [Fig. 5(a)] reproduces the perfect parabolic dispersion found in earlier studies.<sup>7,8</sup> The parabola is centered at the  $\bar{\Gamma}$  point of the surface Brillouin zone and the band bottom is observed at  $E_B = 391(3) \text{ meV}$ . The most significant changes in the data sets from the vicinal surfaces are a shift of the band bottom towards higher kinetic energies and a considerable increase in linewidth with decreasing terrace length. The dispersion remains free electron like. Maximal binding energies of  $E_B^{(332)} = 296(10) \text{ meV}$  and  $E_B^{(221)} = 167(15) \text{ meV}$  are observed at  $k_x = \pi/\langle l \rangle$ . Energy distribution curves at the band bottom are shown in Fig. 6. While the spectrum from Cu(111) shows a narrow Lorentzian line shape the spectra from the vicinal samples are slightly asymmetric and considerably broader. The asymmetry is much more pronounced in the case of Cu(221).

## B. One-dimensional band model

The energy shift of the surface state band bottom has been reported for different Cu surfaces<sup>12–14,18</sup> and was rationalized

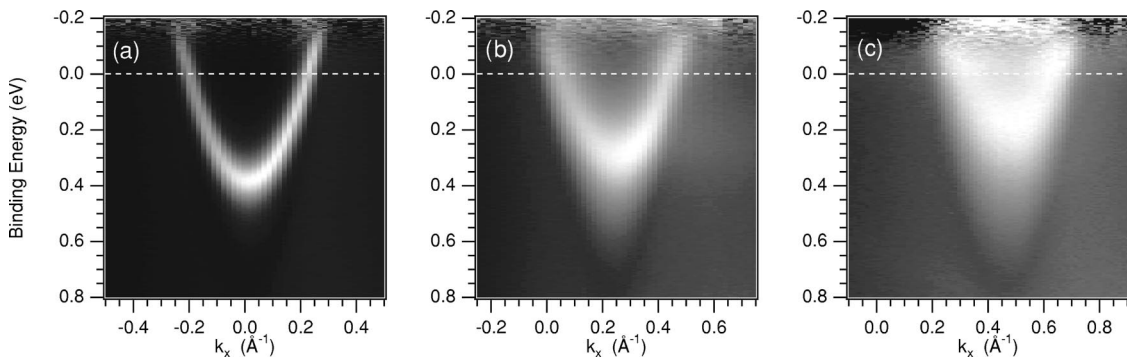


FIG. 5. Angle-scanned energy distribution curves along  $\bar{\Gamma}\bar{M}$  from (a) Cu(111), (b) Cu(332), and (c) Cu(221). The data are normalized with a Fermi-Dirac distribution function and mapped to  $k_x$  according to Eq. (1).

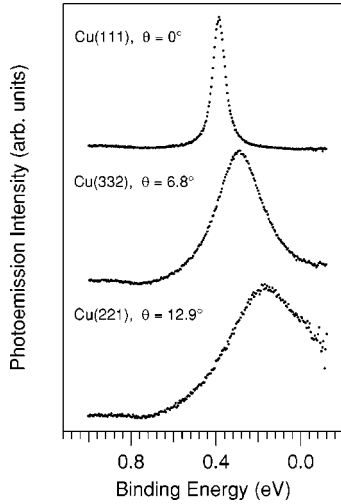


FIG. 6. Energy distribution curves at the band minimum ( $k_x = \pi/\langle l \rangle$ ). The spectra are divided by a Fermi function and normalized to equal peak intensity.

with a 1D Kronig-Penney model that accounts for the effect of the step-induced repulsive potential to the free-electron-like surface state.<sup>14,18</sup> However, for the purpose of the present paper a description in terms of second-order perturbation theory is more convenient. Like the Kronig-Penney analysis in earlier work, we restrict ourselves to a 1D model and include the competing atomic potentials only via an effective mass of the surface state electrons. The application of a 1D model is supported by the measured dispersion along the steps, which is very close to the one on the step free surface. Since the experiment shows free-electron-like dispersing bands, we can use nondegenerate perturbation theory considering only the  $\vec{G}=0$  component of the wave function in the plane-wave expansion ( $\vec{G}$  is a reciprocal lattice vector of the step lattice).<sup>28</sup> Then the energy shift of the band bottom is given by

$$\Delta E_B = U_0 - 2 \sum_{\vec{G}>0} \frac{|U_{\vec{G}}|^2}{\epsilon_1(\vec{G})}, \quad (2)$$

where  $U_{\vec{G}}$  are the Fourier coefficients of the potential and  $\epsilon_1(k) = \hbar^2 k^2 / 2m_0$  is the dispersion of the unperturbed band. To zero order the band shift is given by  $\Delta E_B \approx U_0 [ |U_{\vec{G}}|^2 \ll \epsilon_1(\vec{G}) ]$ , and since  $U_0$  is proportional to the step density, we can write  $\Delta E_B \approx \bar{U}_{step} / \langle l \rangle$ , where  $\bar{U}_{step}$  is the integral over the repulsive step potential as it is obtained in a Kronig-Penney analysis.<sup>14</sup> The quantity which is related to the charge confinement on the terraces, however, is the increase of the effective mass  $m_x$  with respect to the effective mass  $m_0$  of the unperturbed band:

$$m_x = \frac{m_0}{1 - 8 \sum_{\vec{G}>0} \left( \frac{|U_{\vec{G}}|}{\epsilon_1(\vec{G})} \right)^2}. \quad (3)$$

This equation relates the effective mass in the vicinity of the band bottom to the higher Fourier coefficients of the poten-

tial which determine the magnitude of the band gap at the superlattice zone boundaries. Its validity of course is restricted to small potential coefficients and for the limit of a noninteracting electron gas.

### C. Line shape analysis

In a 2D system the energy and momentum distribution of the photocurrent resulting from direct transitions becomes particularly simple.<sup>29</sup> In the small momentum range of interest matrix element effects may be neglected and the photoemission intensity essentially corresponds to the hole spectral function

$$A(k, \epsilon) = \frac{\pi^{-1} \Sigma_I}{(\epsilon - E_i(k) - \Sigma_R)^2 + (\Sigma_I)^2}, \quad (4)$$

where  $\Sigma = \Sigma_R(k, \epsilon) + i \Sigma_I(k, \epsilon)$  denotes the hole self-energy. For weakly interacting systems  $\Sigma_R$  vanishes. Provided the self-energy varies slowly with energy and momentum the direct transition line becomes a Lorentzian at the *initial-state* energy  $E_i(k)$ . The linewidth  $\Gamma$  is related to the lifetime  $\tau$  of the excited photohole by  $\Gamma = 2 \Sigma_I = \hbar / \tau$ .<sup>29</sup> Additional peak broadening can occur due to the finite experimental resolution and for systems with a high defect density.<sup>30,31</sup> Both effects can influence as well the apparent dispersion in an angle-scanned photoemission experiment. In the present study we can neglect the experimental resolution, since it contributes less than 5% to the total linewidths from the vicinal surfaces.

The influence of surface morphology on surface state line shapes was successfully described by approximating the photocurrent as the sum over the spectral functions from an incoherent ensemble.<sup>31,32</sup> For electrons close to the Fermi level the *initial-state* coherence length  $L_i$  is limited by inelastic scattering processes, ensuring thermal equilibrium. The surface state wave function at a vicinal surface may thus be viewed as a wave packet and its wave vector will consequently show a certain distribution following the local direction of the surface. For a quantitative modeling of this effect we make two simplifying assumptions. First we assume that the wave packet averages over an area given by its initial-state coherence length, i.e., that the dispersion does not depend on the details of the probed step sequence. The step lattice, however, shall affect the effective masses as outlined in Eq. (3) and the band bottom shall be pinned in  $k$ -space to  $k_0 = \pi / \bar{l}_i$ , where  $\bar{l}_i$  denotes the average terrace length in the area probed by the surface state. Furthermore, we neglect defects along the steps like e.g., kinks and approximate the spatial averaging by an integration over the width distribution  $P(\bar{l}_i)$  in the continuum limit<sup>33</sup>:

$$I(\epsilon, k_x, k_y) = I_0 \int_{-\infty}^{\infty} d\bar{l}_i P(\bar{l}_i) A(\epsilon, k_x, k_y, E_i), \quad (5)$$

where  $E_i = E_i(k_x, k_y, \bar{l}_i)$  denotes the terrace-length-dependent dispersion relation. As discussed above, we assume a free-electron-like dispersion with different effective masses for motion along and perpendicular to the steps. The

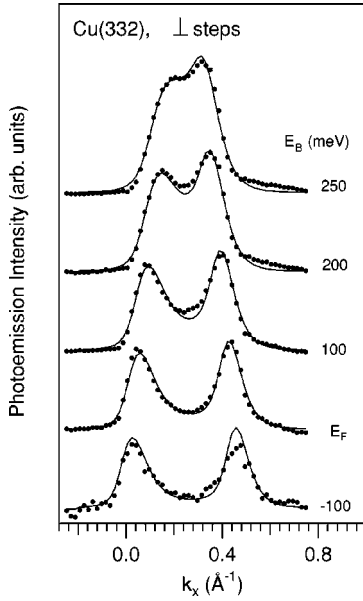


FIG. 7. Momentum distribution curves perpendicular to the steps from Cu(332). The data are normalized with the changing flux on the sample and corrected for a smooth polynomial background. The thin lines are the results of a 2D fit using Eq. (5).

only terrace-length-dependent quantities are the energy and momentum shift of the band bottom:

$$E(k_x, k_y, \bar{l}_i) = E_0^{(111)} + \frac{\bar{U}_{step}}{\bar{l}_i} + \frac{\hbar^2(k_x - \pi/\bar{l}_i)^2}{2m_x} + \frac{\hbar^2 k_y^2}{2m_y}. \quad (6)$$

Inserting Eq. (6) in Eq. (5) we obtain an expression for the photocurrent in energy-momentum space as a function of six parameters. Three of them, namely, the potential offset  $\bar{U}_{step}$  and the two effective masses  $m_x, m_y$ , describe the initial-state dispersion which we are primarily interested in. Surface morphology enters via the width distribution  $P(\bar{l}_i)$  which is sharper than the distribution of single terraces  $P(l)$  if the surface state averages over several consecutive terraces. If we approximate the terrace width distribution by a Gaussian with standard deviation  $\sigma_{\bar{l}_i}$ ,  $P(\bar{l}_i)$  will be Gaussian as well and its standard deviation  $\sigma_{\bar{l}_i}$  is related to the initial-state coherence length by  $L_i = (\sigma_{\bar{l}_i}/\sigma_{\bar{l}_i})^2 \langle l \rangle$ . Fitting  $P(\bar{l}_i)$  to the experiment can thus give an estimate on  $L_i$ . The hole many-body physics finally is covered by  $\Sigma_I$ .

Since some of the parameters are correlated and since neither energy distribution curves (EDC's) nor momentum distribution curves (MDC's) are sensitive to all fit parameters, we performed two-dimensional fits in both planes of measurement. A set of MDC's from Cu(332) for different binding energies as extracted from the data in Fig. 5(b), together with the corresponding fits is displayed in Fig. 7. The fit parameters are summarized in Table I. The excellent agreement between fit and data is achieved with a constant self-energy of  $2\Sigma_I = 190$  meV. In particular the different line shapes of the two peaks are well reproduced by the fits.

TABLE I. Surface-state band parameters, as obtained from the 2D fits with Eq. (5). The values for  $m_y/m_x$  are averaged from different data sets from the same samples.  $\sigma_{\bar{l}_i}$  denotes the standard deviation of the terrace width distribution sampled by the surface-state. The morphology parameters from the LEED analysis are added in brackets for comparison.

	Cu(111)	Cu(332)	Cu(221)
$\bar{U}_{step}$ (eV Å)	–	1.09	1.52
$m_x$ ( $m_e$ )	0.41(2)	0.45(3)	0.49(5)
$m_y/m_x$	1.00(1)	0.87(7)	1.05(12)
$2\Sigma_I$ (meV)	54 <sup>a</sup>	190	300
$\langle l \rangle^{ARUPS} [\langle l \rangle^{LEED}]$ (Å)	–	12.6 [12.7]	6.7 [7.0]
$\sigma_{\bar{l}_i}^{ARUPS} [\sigma_{\bar{l}_i}^{LEED}]$ (Å)	–	0.17 [0.31]	0.06 [0.30]

<sup>a</sup>Reference 34.

The same parameter set was used to fit the Cu(332) FSM with the only free parameter being the effective mass for motion along the steps. We find good agreement between fit and data for an anisotropy  $m_y/m_x$  of 0.87 as can be judged from the extracted MDC's, shown in Fig. 8. The peak shape is well represented with the same self-energy and morphology parameter used to fit the  $(k_x, E)$  plane. The analysis of different constant energy surfaces down to binding energies of 0.22 eV shows no energy dependence of  $m_y/m_x$ . The values for the anisotropy depend critically on the width distribution  $P(\bar{l}_i)$ . If we hold the standard deviation  $\sigma_{\bar{l}_i}$  at zero, corresponding to perfect surface order, we obtain  $m_y/m_x = 0.65$ , considerably different from the best fit.  $P(\bar{l}_i)$ , however, affects as well the asymmetry of the MDC's and the variations in the linewidths. Since the three distinctly different line shapes in the Fermi level crossing from Cu(332) are well reproduced by the fits, we expect the determined anisot-

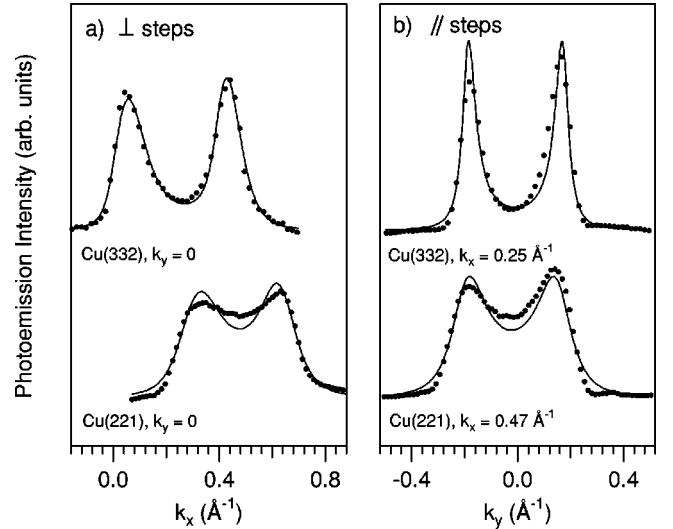


FIG. 8. Momentum distribution curves at the Fermi level perpendicular to the steps (a) and along the steps (b). The data are shown in the correct intensity ratio. Note that the different linewidths of the Fermi level crossings are described with a  $k$ -independent self-energy.

ropy to be highly reliable. An error of 0.07 is estimated from the spread in different data sets from the same sample. For  $\sigma_{\bar{l}_i}$  we find a value of 0.17. From a comparison with  $\sigma_l = 0.31\langle l \rangle$  as obtained by LEED for the distribution of single terraces we estimate an initial state coherence length  $L_i$  of the order of three terraces.

The agreement between fit and data is less satisfactory for Cu(221). This is surprising since we expect that the dispersion in Eq. (6) is more appropriate for Cu(221), where  $k_F$  is far from the zone boundary and might indicate the limitations of the present analysis. The main results, however, can be observed in the raw data as well. The FSM is highly isotropic and shows a broad rather symmetric peak in the MDC's with a weak momentum dependence of the linewidth. This indicates a small anisotropy and a reduced sensitivity to the width distribution  $P(\bar{l}_i)$ , which is confirmed by the fits.

#### D. Discussion

With the presented results, the scenario of a continuous surface state to surface resonance transition emerges. This transition is driven by the closing of the projected band gap, which allows hybridization of surface and bulk states. This is supported by the strong increase in linewidth with increasing miscut away from the [111] direction. The fit results using the presented line shape model indicate that approximately 2/3 of the smaller high binding energy side half width at half maximum at  $\bar{M}_{1/2,0}$  can be attributed to lifetime broadening, 1/3 to inhomogeneous broadening due to the terrace width distribution. The importance of the different decay channels of the photohole can be estimated from a comparison with the well-characterized Cu(111) surface.<sup>35-37</sup> The room-temperature linewidth on flat Cu(111) can be decomposed into a temperature-dependent electron-phonon contribution  $\Gamma_{e-ph} \approx 16$  meV and a low-temperature linewidth of  $\approx 20$  meV which has been attributed predominantly to intraband transitions.<sup>37</sup> Decay of the photohole within the surface state band should not depend significantly on the miscut angle. Electron-phonon coupling is expected to increase with increasing bulk penetration of the surface state wave function.<sup>38</sup> It might increase as well due to quasielastic scattering at steps. However, the observed linewidths of  $\Gamma^{(332)} \approx 190$  meV and  $\Gamma^{(221)} \approx 300$  meV cannot be explained with a reasonable coupling parameter. It is therefore compelling to attribute the dominant decay channel on the vicinal surfaces to the scattering of the photohole with bulk electrons near the surface as it is expected for a surface resonance.

The effective step potential can be estimated from the anisotropy in the Fermi surface. With the assumption of an unperturbed propagation parallel to the steps the potential coefficients are readily calculated using Eq. (3). In the case of Cu(221) we see no significant difference between  $m_x$  and  $m_y$ . Consequently the higher Fourier coefficients  $U_{\vec{G}>0}$  are compatible with zero, indicating a very small spatial variation of the effective potential. However, the spread in different data sets from the same sample is too large to determine a significant upper limit. For Cu(332) we obtain  $\Sigma[U_{\vec{G}}/\epsilon_1(\vec{G})]^2 = 0.016$  by inserting  $m_y/m_x^{(332)} = 0.87$  into

Eq. (3). In the limiting case of a  $\delta$ -function potential all  $U_{\vec{G}>0}$  are equal and thus readily calculated to be  $U_{\vec{G}>0} = 0.28$  eV. Here  $U_0 = 0.16$  eV is obtained by inserting  $\Delta E = 95$  meV into Eq. (2). However, these coefficients are not small compared with the unperturbed bandwidth in the step lattice of  $E_1 \sim 0.55$  eV. Thus the approximations made to deduce the Eqs. (2) and (3) are no longer valid. An exact solution of the periodic array of  $\delta$  potentials, chosen such as to reproduce the experimental effective masses,<sup>39</sup> however, results in a dispersion very close to the one obtained with perturbation theory. It reproduces in particular the unrealistically large band gap of  $E_g = 2U_1 \sim 0.55$  eV and the narrow bandwidth of  $E_1 \sim 0.3$  eV, which is considerably smaller than the experimental value of  $E_1^{(332)} > 0.4$  eV. These unrealistic predictions indicate the limited validity of the applied 1D band structure model. In particular an anisotropic coherence length and disorder in the step lattice may influence the dispersion as well. These effects may also reduce or even completely fill the predicted band gap at the superlattice zone boundary.

#### IV. SUMMARY

In a comparative study we characterized the surface state dispersion on Cu(111) and the vicinal Cu(332) and Cu(221) surfaces using angle-scanned ultraviolet photoemission. We find on both vicinal surfaces a 2D surface state, coherently interacting over several terraces. The finite width of the terrace size distribution is found to influence the spectra considerably. To extract the intrinsic initial-state dispersion from the data, we used a simple model including the spatial averaging as a 1D integral over the terrace width distribution. With this analysis we can quantify the anisotropy in the dispersion for motion along and perpendicular to the steps. In the case of Cu(332) we find a considerable deviation from the isotropic Fermi surface of a free-electron gas. This is evidence for the Bloch nature of the surface state in the periodic step lattice and provides an estimate of the effective step potential. The reduced sensitivity to the step potentials found on Cu(221) can be explained by the enhanced hybridization with bulk states leading to a larger bulk penetration of the surface state. It might be related as well to the increasing overlap between neighboring step potentials and the disappearance of the 1D state found on Cu(332).<sup>16</sup> The enhanced surface-bulk coupling explains as well the decreasing photohole lifetime with increasing step density as obtained from the line shape analysis. The strong angle dependence of the linewidth, however, is conveniently explained with the spatial averaging and gives no indications of a momentum dependence of the hole self-energy as could arise from an anisotropic step related electron-electron or electron-phonon interaction.

#### ACKNOWLEDGMENTS

We thank R. Monnier and M. Hengsberger for fruitful discussions and S. Speller for the provision of Ref. 26 prior to publication. This work was supported by the Swiss National Science Foundation.

- <sup>1</sup>J.W.M. Frenken and P. Stoltze, Phys. Rev. Lett. **82**, 3500 (1999).
- <sup>2</sup>M. Salmeron, R.J. Gale, and G.A. Somorjai, Chem. Phys. **67**, 5324 (1977).
- <sup>3</sup>T. Zambelli, J. Trost, J. Wintterlin, and G. Ertl, Phys. Rev. Lett. **76**, 795 (1996).
- <sup>4</sup>F.J. Himpsel, T. Jung, and J.E. Ortega, Surf. Rev. Lett. **4**, 371 (1997).
- <sup>5</sup>J. Shen, R. Skomski, M. Klaua, H. Jenniches, S. Sundar Manoharan, and J. Kirschner, Phys. Rev. B **56**, 2340 (1997).
- <sup>6</sup>W. Shockley, Phys. Rev. **56**, 317 (1939).
- <sup>7</sup>P.O. Gartland and B.J. Slagsvold, Phys. Rev. B **12**, 4047 (1975).
- <sup>8</sup>S.D. Kevan and R.H. Gaylord, Phys. Rev. B **36**, 5809 (1987).
- <sup>9</sup>N.V. Smith, Phys. Rev. B **32**, 3549 (1985).
- <sup>10</sup>M.F. Crommie, C.P. Lutz, and D.M. Eigler, Nature (London) **363**, 524 (1993).
- <sup>11</sup>J. Repp, F. Moresco, G. Meyer, K.H. Rieder, P. Hyldgaard, and M. Persson, Phys. Rev. Lett. **85**, 2981 (2000).
- <sup>12</sup>R.S. Williams, P.S. Wehner, S.D. Kevan, R.F. Davis, and D.A. Shirley, Phys. Rev. Lett. **41**, 323 (1978).
- <sup>13</sup>A.P. Shapiro, T. Miller, and T.C. Chiang, Phys. Rev. B **38**, 1779 (1988).
- <sup>14</sup>O. Sánchez, J.M. García, P. Segovia, J. Alvarez, A.L. Vázquez de Parga, J.E. Ortega, M. Prietsch, and R. Miranda, Phys. Rev. B **52**, 7894 (1995).
- <sup>15</sup>J.E. Ortega, S. Speller, A.R. Bachmann, A. Mascaraque, E.G. Michel, A. Närmann, A. Mugarza, A. Rubio, and F.J. Himpsel, Phys. Rev. Lett. **84**, 6110 (2000).
- <sup>16</sup>F. Baumberger, T. Greber, and J. Osterwalder, Phys. Rev. B **62**, 15 431 (2000).
- <sup>17</sup>R. Paniago, R. Matzdorf, G. Meister, and A. Goldmann, Surf. Sci. **336**, 113 (1995).
- <sup>18</sup>M. Hengsberger, D. Purdie, M. Garnier, K. Breuer, and Y. Baer, Surf. Sci. **405**, 491 (1998).
- <sup>19</sup>X.Y. Wang, X.J. Shen, R.M. Osgood, Jr., R. Haight, and F.J. Himpsel, Phys. Rev. B **53**, 15 738 (1996).
- <sup>20</sup>P. Aebi, J. Osterwalder, R. Fasel, D. Naumovic, and L. Schlapbach, Surf. Sci. **307-309**, 907 (1994).
- <sup>21</sup>M. Lindroos and A. Bansil, Phys. Rev. Lett. **77**, 2985 (1996).
- <sup>22</sup>J. Osterwalder, Surf. Rev. Lett. **4**, 391 (1996).
- <sup>23</sup>T. Greber, O. Raetz, T.J. Kreutz, P. Schwaller, W. Deichmann, E. Wetli, and J. Osterwalder, Rev. Sci. Instrum. **68**, 4549 (1997).
- <sup>24</sup>M. Hoesch, diploma thesis, University of Zurich, 1998.
- <sup>25</sup>J. Wollschläger, Surf. Sci. **383**, 103 (1997).
- <sup>26</sup>A. R. Bachmann, A. Mugarza, J. E. Ortega, A. Närmann, and S. Speller (unpublished).
- <sup>27</sup>R. Matzdorf and A. Goldmann, Surf. Sci. **400**, 329 (1998).
- <sup>28</sup>N. W. Ashcroft and N. D. Mermin, *Solid State Physics* (Holt-Saunders International, New York, 1976).
- <sup>29</sup>N.V. Smith, P. Thiry, and Y. Petroff, Phys. Rev. B **47**, 15 476 (1993).
- <sup>30</sup>A. Beckmann, K. Meinel, Ch. Ammer, M. Heiler, and H. Neddermeyer, Surf. Sci. **375**, L363 (1997).
- <sup>31</sup>Th. Fauster, Ch. Reuss, I.L. Shumay, M. Weinelt, F. Theilmann, and A. Goldmann, Phys. Rev. B **61**, 16 168 (2000).
- <sup>32</sup>A. Beckmann, C. Ammer, K. Meinel, and H. Neddermeyer, Surf. Sci. **432**, L589 (1999).
- <sup>33</sup>A similar equation was derived by Beckmann *et al.* (Ref. 32) to describe the line shape of a Tamm state on vicinal Cu(100). There, however, the integration was carried out over the width distribution of single terraces, rather than the average terrace length in the region probed by the surface state.
- <sup>34</sup>Our value of  $2\sum_l = 54$  meV is obtained by fitting a Lorentzian convolved with a Gaussian of 31 meV FWHM to the low-energy side of the spectrum. The total linewidth amounts to 68 meV. Very recent measurements at the highest resolution interpolate to a room-temperature linewidth of  $\sim 36$  meV: G. Nicolay and F. Reinert (private communication).
- <sup>35</sup>B.A. McDougall, T. Balasubramanian, and E. Jensen, Phys. Rev. B **51**, 13 891 (1995).
- <sup>36</sup>G. Nicolay and F. Reinert (private communication); F. Reinert, G. Nicolay, S. Schmidt, D. Ehm, and S. Hüfner, Phys. Rev. B **63**, 115415 (2001).
- <sup>37</sup>J. Kliewer, R. Berndt, E.V. Chulkov, V.M. Silkin, P.M. Echenique, and S. Crampin, Science **288**, 1399 (2000).
- <sup>38</sup>R. Matzdorf, G. Meister, and A. Goldmann, Phys. Rev. B **54**, 14 807 (1996).
- <sup>39</sup>In a Kronig-Penney model the shift of the band bottom is given by  $\Delta E = U_0 a / l$  where  $U_0 a$  is the integral over the potential barrier. To adjust the energy of the band bottom we used a potential of the form  $U(x) = U_0 + U_s a \delta(x - nl)$  with  $U_s a \sim 3.5$  eV Å and  $U_0 = -0.17$  eV.